Control and optimization of solute transport in a thin porous tube

I. M. Griffiths, P. D. Howell, and R. J. Shipley

Citation: Physics of Fluids **25**, 033101 (2013); doi: 10.1063/1.4795545

View online: http://dx.doi.org/10.1063/1.4795545

View Table of Contents: http://scitation.aip.org/content/aip/journal/pof2/25/3?ver=pdfcov

Published by the AIP Publishing

PHYSICS OF FLUIDS **25**, 033101 (2013)

Control and optimization of solute transport in a thin porous tube

I. M. Griffiths,[1,a)] P. D. Howell,[2] and R. J. Shipley[3]
[1]*Oxford Centre for Collaborative Applied Mathematics, Mathematical Institute, University of Oxford, Oxford, Oxfordshire OX1 3LB, United Kingdom*
[2]*Oxford Centre for Industrial Applied Mathematics, Mathematical Institute, University of Oxford, Oxford, United Kingdom*
[3]*Department of Mechanical Engineering, University College London, London, United Kingdom*

(Received 23 November 2012; accepted 1 March 2013; published online 26 March 2013)

Predicting the distribution of solutes or particles in flows within porous-walled tubes is essential to inform the design of devices that rely on cross-flow filtration, such as those used in water purification, irrigation devices, field-flow fractionation, and hollow-fibre bioreactors for tissue-engineering applications. Motivated by these applications, a radially averaged model for fluid and solute transport in a tube with thin porous walls is derived by developing the classical ideas of Taylor dispersion. The model includes solute diffusion and advection via both radial and axial flow components, and the advection, diffusion, and uptake coefficients in the averaged equation are explicitly derived. The effect of wall permeability, slip, and pressure differentials upon the dispersive solute behaviour are investigated. The model is used to explore the control of solute transport across the membrane walls via the membrane permeability, and a parametric expression for the permeability required to generate a given solute distribution is derived. The theory is applied to the specific example of a hollow-fibre membrane bioreactor, where a uniform delivery of nutrient across the membrane walls to the extra-capillary space is required to promote spatially uniform cell growth.
 [http://dx.doi.org/10.1063/1.4795545]

I. INTRODUCTION

Transport of solutes or particles in a flow within a porous-walled tube is a key feature of many natural, industrial, and biological systems, such as groundwater flows, fluidized beds, and blood flows in the body. The porosity of the walls is also a feature that is exploited in numerous filtration and separation systems, in particular cross-flow filtration and field-flow fractionation (FFF) devices. In both scenarios, the objective is to separate particulates or molecules from a bulk fluid. Cross-flow filtration achieves this by pumping fluid containing suspended particles or dissolved solute down a tube with porous walls (also referred to as a membrane), and is used in a broad set of applications including water purification, protein separation for gene therapies, soluble antibiotic extraction, blood fractionation, and tissue-engineering bioreactors.[1–5] By controlling the membrane permeability and pressure drop down the tube relative to that across the membrane, the proportion of fluid that permeates across the membrane can be prescribed. This enables separation of particles that are too large to pass through the membrane pores (for example, in water purification processes), as well as controlled delivery of solutes to the extra-membrane space (such as in tissue-engineering applications).

By comparison hollow-fibre FFF employs a similar set-up to cross-flow filtration, but imposes a secondary flow to enable further control of the separation process. Particles are separated according to

[a)]Electronic mail: ian.griffiths@maths.ox.ac.uk

the axial position at which they penetrate the porous membrane, and again the membrane permeability is a key parameter that enables control of the particles trajectories and separation efficiency. Due to the tighter control that is enabled, FFF is used in the separation and size characterization of particulates, water-soluble polymers, and biological macromolecules,[6–8] and has generated recent interest.[9]

In order to maximize the capability and efficiency of the processes described above, it is essential to understand and exploit the relationship between the controllable quantities (such as the wall permeability) and the consequent distribution of particles or solute. For example, tissue-engineering bioreactors aim to control cell population growth through nutrient delivery. Spatially homogeneous nutrient delivery will promote spatially uniform growth, and it is fundamentally important to understand how to control the bioreactor operation to achieve this. Crucially the membrane permeability can be tuned spatially by changing the operating parameters of the fabrication process. The requirement of spatial uniformity in solute distribution also extends to larger scale configurations such as in commercial irrigation devices,[10] where an approximately even distribution of the plant nutrient that is injected into the irrigation system is desired.

The control of solute distribution is also an important feature in filtration devices. The distribution of filtrate material plays a key role in membrane fouling through a range of mechanisms including pore blocking, pore constriction, and/or caking. These processes change the effective membrane properties and lead to a reduction in the overall filtration efficiency—a key challenge is to understand how to both reduce and predict the effect of fouling on membrane function. This is particularly relevant in cases where the solute costs are extremely high and thus it is essential to minimize loss of the solute to the membrane. One example involves the delivery of growth factors in tissue-engineering bioreactors.[11] Growth factors are proteins that are essential to maintain cell function and are extremely costly; when delivered to a cell population via a membrane, it is vital to minimize wastage of these factors through membrane fouling, so that the resulting system is cost-efficient to operate.

Understanding solute transport is clearly fundamentally important in shaping the design of the systems described above. A range of experimental and numerical tools has been used to investigate filtration devices.[12–15] However, it remains rare to relate the dispersive effects that occur when a solute spreads within a flow field to device design. For instance, Doshi *et al.* investigate solute dispersion in a uniform suction flow field,[16] although the impact of membrane permeability on the solutal distribution has not been considered, to the best of our knowledge.

In this paper we develop a mathematical model for solute transport in a tube with porous walls, where the wall Darcy permeability may vary spatially. We begin in Sec. II by considering the specific example of a flow generated by a uniform volume flux of fluid injected at the inlet, while the outlet is maintained at a constant pressure (these conditions are typical of those used to operate many filtration and hollow-fibre bioreactor (HFB) devices). Next a solute transport model that includes advection via both radial and axial flow components, as well as diffusion, is presented in Sec. III. In Sec. IV we exploit the small aspect ratio of the tube (and thin membrane compared to the tube radius) to derive a simplified one-dimensional asymptotic system that characterizes the dispersive behaviour of the solute within the tube flow. The radial flow that is generated as a result of the wall permeability provides a novel generalization of the classical Taylor-dispersion theory that holds for an impermeable tube or a tube with uniform suction.

In Sec. V the dispersion of a localized pulse of solute injected into either an infinitely long or finite-length tube is investigated. The solute concentration will invariably be highest where it is injected at the inlet, and will fall as it moves downstream, introducing heterogeneity in supply across the membrane. With this in mind, in Sec. VI we investigate the effect of wall permeability on the solute distribution across the membrane. The simplified Taylor-dispersion model derived lends itself to a clear analysis of the precise system behaviour and thus allows for a better understanding of the influence of the membrane permeability on the solute dispersion and transport. We use this to derive (a) an expression for the solute distribution generated by a uniform permeability and (b) the spatial variation in the membrane permeability required to generate a prescribed spatial solute distribution. Finally we explore the specific example of a spatially homogeneous solute distribution

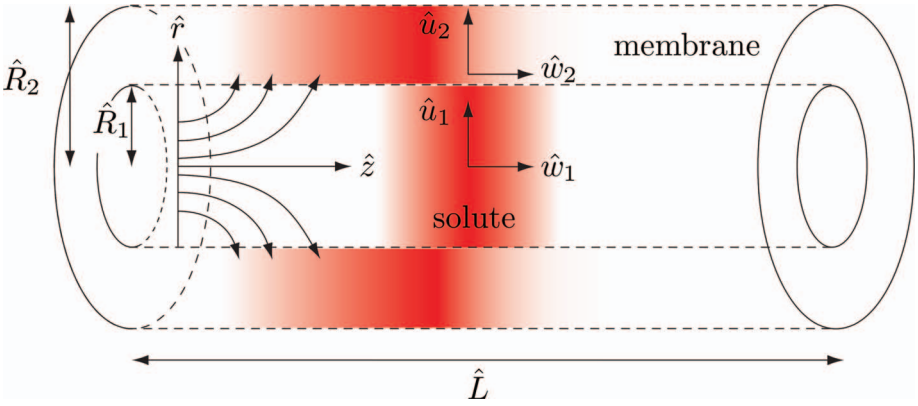

FIG. 1. Schematic diagram for the solute flow in a porous tube.

in a tissue-engineering bioreactor, with the objective of stimulating uniform cell population growth from a single pulse of nutrient.

The implications of the theory presented are discussed in Sec. VII and conclusions are drawn.

II. FLUID TRANSPORT MODEL

We consider the transport of fluid in a tube of radius $\hat{R}_1$ and characteristic length $\hat{L}$, surrounded by a porous membrane with outer radius $\hat{R}_2$, as illustrated in Figure 1. Assuming an axisymmetric set-up, we denote the radial and axial directions by $\hat{r}$ and $\hat{z}$, with corresponding velocity components $\hat{u}_1$, $\hat{w}_1$ in the pipe and $\hat{u}_2$, $\hat{w}_2$ in the membrane. We assume a small aspect ratio geometry and that the membrane is thin in comparison to the pipe radius, so that

$$\frac{\hat{R}_1}{\hat{L}} = \epsilon \ll 1, \tag{1a}$$

$$\frac{\hat{R}_2 - \hat{R}_1}{\hat{R}_1} = \delta \ll 1. \tag{1b}$$

Assuming slow viscous flow in the pipe, the velocity is described by the axisymmetric Stokes equations for an incompressible, Newtonian fluid of constant viscosity,

$$\frac{1}{\hat{r}}\frac{\partial}{\partial \hat{r}}(\hat{r}\hat{u}_1) + \frac{\partial \hat{w}_1}{\partial \hat{z}} = 0, \tag{2a}$$

$$\frac{\partial \hat{p}_1}{\partial \hat{r}} = \hat{\mu}\left[\frac{1}{\hat{r}}\frac{\partial}{\partial \hat{r}}\left(\hat{r}\frac{\partial \hat{u}_1}{\partial \hat{r}}\right) + \frac{\partial^2 \hat{u}_1}{\partial \hat{z}^2} - \frac{\hat{u}_1}{\hat{r}^2}\right], \tag{2b}$$

$$\frac{\partial \hat{p}_1}{\partial \hat{z}} = \hat{\mu}\left[\frac{1}{\hat{r}}\frac{\partial}{\partial \hat{r}}\left(\hat{r}\frac{\partial \hat{w}_1}{\partial \hat{r}}\right) + \frac{\partial^2 \hat{w}_1}{\partial \hat{z}^2}\right], \tag{2c}$$

where $\hat{p}_1$ and $\hat{\mu}$ are the fluid pressure and dynamic viscosity, respectively. The fluid velocity in the membrane $(\hat{u}_2, \hat{w}_2)$ is described by Darcy's law for a porous medium with constant porosity,

$$\frac{1}{\hat{r}}\frac{\partial}{\partial \hat{r}}(\hat{r}\hat{u}_2) + \frac{\partial \hat{w}_2}{\partial \hat{z}} = 0, \tag{2d}$$

$$\hat{u}_2 = -\frac{\hat{k}(\hat{z})}{\hat{\mu}}\frac{\partial \hat{p}_2}{\partial \hat{r}}, \quad \hat{w}_2 = -\frac{\hat{k}(\hat{z})}{\hat{\mu}}\frac{\partial \hat{p}_2}{\partial \hat{z}}. \tag{2e}$$

Here $\hat{p}_2$ is the fluid pressure in the membrane and $\hat{k}$ is the Darcy permeability of the membrane to fluid transport. Here we suppose that $\hat{k}$ may vary with axial distance $\hat{z}$, as a consequence of the manufacturing process, but not time, and that the flow field is steady. (In practice a membrane material will be anisotropic but since the membrane is thin we may assume variations in the radial direction are negligible.)

We apply continuity of fluid flux and pressures, and an appropriate slip condition at the pipe–membrane interface:[17]

$$\hat{u}_1 = \hat{\phi}\hat{u}_2, \tag{3a}$$

$$\hat{p}_1 = \hat{p}_2, \tag{3b}$$

$$\frac{\partial \hat{w}_1}{\partial \hat{r}} = -\frac{\hat{\alpha}}{\sqrt{\hat{k}}}(\hat{w}_1 - \hat{w}_2) \tag{3c}$$

on $\hat{r} = \hat{R}_1$, where $\hat{\phi}$ is the membrane porosity (assumed constant) and $\hat{\alpha}$ is a dimensionless parameter that quantifies the slip. We suppose that outside the membrane the fluid is at atmospheric pressure, $\hat{p}_{\text{atm}}$, so that continuity of fluid pressure at the interface between the membrane and the surroundings gives

$$\hat{p}_2 = \hat{p}_{\text{atm}}, \qquad \text{on} \quad \hat{r} = \hat{R}_2. \tag{3d}$$

The system is closed by prescribing the pressure at the tube outlet ($\hat{z} = \hat{L}$) and the mean axial velocity at the tube inlet ($\hat{z} = 0$),

$$\frac{2}{\hat{R}_1^2}\int_0^{\hat{R}_1} \hat{r}\hat{w}_1(\hat{r}, 0)\,\mathrm{d}\hat{r} = \hat{W}, \tag{3e}$$

which is prescribed experimentally and assumed constant.

We adopt a lubrication approach, exploiting the small aspect ratio ϵ defined by (1a), by non-dimensionalizing lengths via

$$\hat{r} = \epsilon\hat{L}r, \qquad \hat{z} = \hat{L}z, \tag{4a}$$

in the pipe, and

$$\hat{r} = \hat{R}_1 + \delta\hat{R}_1\eta, \tag{4b}$$

in the membrane. To ensure the richest asymptotic limit we rescale the porosity, $\hat{\phi} = \epsilon\delta\phi$. The appropriate scalings for the velocity components and time are then

$$\hat{w}_i = \hat{W}w_i, \qquad \hat{u}_1 = \epsilon\hat{W}u_1, \qquad \hat{u}_2 = \frac{1}{\delta}\hat{W}u_2, \qquad \hat{t} = \frac{\hat{L}}{\hat{W}}t, \tag{4c}$$

for $i = 1, 2$. We also scale the pressures in the pipe and membrane via

$$\hat{p}_1 = \hat{p}_{\text{atm}} + \frac{\hat{\mu}\hat{W}}{\epsilon^2\hat{L}}p_1, \qquad \hat{p}_2 = \hat{p}_{\text{atm}} + \frac{\hat{\mu}\hat{W}}{\epsilon^2\hat{L}}p_2, \tag{5}$$

where p_{atm} denotes atmospheric pressure. The natural scaling for the wall permeability is then,

$$\hat{k} = \epsilon^3\hat{L}^2k. \tag{6}$$

First of all, we consider fluid transport in the membrane. To leading order in δ, the dimensionless counterpart to the continuity equation (2d) gives

$$\frac{\partial u_2}{\partial \eta} = 0, \tag{7}$$

as would be expected for a thin-membrane regime, and therefore u_2 is constant within the membrane. The dimensionless axial and radial velocity components are given by

$$u_2 = -k(z)\frac{\partial p_2}{\partial \eta}, \tag{8a}$$

$$w_2 = -\epsilon k(z)\frac{\partial p_2}{\partial z}. \tag{8b}$$

Integrating (8a) with respect to η and applying the dimensionless version of (3d) yields

$$p_2 = -\frac{1}{k}u_2(\eta - 1), \tag{9}$$

while (8b) shows that $w_2 = 0$ across the membrane to leading order in ϵ.

The leading-order dimensionless versions of (2) and (3) implies that $p_1 = p_1(z)$ and

$$\frac{1}{r}\frac{\partial}{\partial r}(ru_1) + \frac{\partial w_1}{\partial z} = 0, \tag{10a}$$

$$\frac{\mathrm{d}p_1}{\mathrm{d}z} = \frac{1}{r}\frac{\partial}{\partial r}\left(r\frac{\partial w_1}{\partial r}\right). \tag{10b}$$

Equations (10a) and (10b) must be solved subject to the boundary conditions

$$2\int_0^1 r w_1(r,0)\,\mathrm{d}r = 1, \tag{10c}$$

$$u_1 = \phi u_2, \tag{10d}$$

$$\frac{\partial w_1}{\partial r} = -A(z)w_1, \tag{10e}$$

$$p_1 = p_2, \ \text{on } r = 1, \ \eta = 0, \tag{10f}$$

where

$$A(z) = \frac{\alpha}{\sqrt{k(z)}} \tag{11}$$

and $\alpha = \hat{\alpha}/\sqrt{\epsilon}$. The parameter A provides a measure of the slip at the membrane interface, weighted against the permeability. It is simple to show that the solution to the system (10) is given by

$$u_1 = -\frac{1}{16A}\frac{\mathrm{d}^2 p_1}{\mathrm{d}z^2}r(Ar^2 - 2A - 4) - \frac{\mathrm{d}p_1}{\mathrm{d}z}\frac{\mathrm{d}A}{\mathrm{d}z}\frac{r}{4A^2}, \tag{12a}$$

$$w_1 = \frac{1}{4A}\frac{\mathrm{d}p_1}{\mathrm{d}z}\left(Ar^2 - A - 2\right), \tag{12b}$$

while the pressure satisfies

$$\frac{\mathrm{d}^2 p_1}{\mathrm{d}z^2} = \frac{16\phi\alpha^2}{A(A+4)}p_1 + \frac{4}{A(A+4)}\frac{\mathrm{d}A}{\mathrm{d}z}\frac{\mathrm{d}p_1}{\mathrm{d}z}. \tag{13}$$

Equations (12) and (13) are a generalization of results of Berman[18] and Shipley *et al.*,[4,19] to account for a spatially dependent wall permeability.

Prescribing the input velocity, (10c), translates to the boundary condition

$$\frac{\mathrm{d}p_1(0)}{\mathrm{d}z} = -\frac{8A(0)}{A(0)+4}, \tag{14}$$

using (12b), and the system (13) is closed by applying an appropriate pressure condition at the outlet.

III. SOLUTE TRANSPORT MODEL

The solute concentrations (per unit volume of fluid) within the pipe and membrane are denoted $\hat{c}_1$ and $\hat{c}_2$, respectively, and are governed by the advection–diffusion equations

$$\frac{\partial \hat{c}_i}{\partial \hat{t}} + \frac{\partial (u_i \hat{c}_i)}{\partial \hat{r}} + \frac{\partial (\hat{w}_i \hat{c}_i)}{\partial \hat{z}} = \frac{\hat{D}_i}{\hat{r}} \frac{\partial}{\partial \hat{r}} \left(\hat{r} \frac{\partial \hat{c}_i}{\partial r} \right) + \hat{D}_i \frac{\partial^2 \hat{c}_i}{\partial \hat{z}^2}, \tag{15}$$

where $i = 1, 2$. Here $\hat{D}_1$ and $\hat{D}_2$ are the solute diffusivities within the pipe and membrane, respectively, and are assumed to be constant.

The appropriate boundary conditions at the pipe–membrane interface will depend on the specific application, however, here we choose to apply continuity of solute concentration and total solute flux, defined as $\hat{\mathcal{Q}}$, which describe a broad range of filtration configurations. Mathematically, these conditions read

$$\hat{c}_1 = \hat{c}_2, \tag{16a}$$

$$\hat{\mathcal{Q}} = \hat{u}_1 \hat{c}_1 - \hat{D}_1 \frac{\partial \hat{c}_1}{\partial \hat{r}} = \hat{\phi} \left(\hat{u}_2 \hat{c}_2 - \hat{D}_2 \frac{\partial \hat{c}_2}{\partial \hat{r}} \right), \tag{16b}$$

on $\hat{r} = \hat{R}_1$. Here $\hat{u}_i \hat{c}_i$ and $\hat{D}_i \partial \hat{c}_i / \partial \hat{r}$ correspond, respectively, to the advective and diffusive transport of the solute out of the pipe ($i = 1$) and into the membrane ($i = 2$). We suppose that there is no solute in the bath of fluid surrounding the membrane, so that

$$\hat{c}_2 = 0 \text{ on } \hat{r} = \hat{R}_2. \tag{17}$$

The non-dimensionalization (4) is applied to (15), with $\hat{c}_i = \hat{c}_0 c$, where $\hat{c}_0$ is a typical solute concentration, which leads to

$$\epsilon Pe_1 \left(\frac{\partial c_1}{\partial t} + u_1 \frac{\partial c_1}{\partial r} + w_1 \frac{\partial c_1}{\partial z} \right) = \frac{1}{r} \frac{\partial}{\partial r} \left(r \frac{\partial c_1}{\partial r} \right) + \epsilon^2 \frac{\partial^2 c_1}{\partial z^2}, \tag{18a}$$

$$\delta^2 \epsilon Pe_2 \frac{\partial c_2}{\partial t} + u_2 \frac{\partial c_2}{\partial \eta} + \delta^2 \epsilon w_2 \frac{\partial c_2}{\partial z} = \frac{1}{1 + \delta \eta} \frac{\partial}{\partial \eta} \left((1 + \delta \eta) \frac{\partial c_2}{\partial \eta} \right) + \epsilon^2 \delta^2 \frac{\partial^2 c_2}{\partial z^2}, \tag{18b}$$

where $Pe_i = \hat{W} \hat{R}_1 / \hat{D}_i$ is the Péclet number of the pipe ($i = 1$) and of the membrane ($i = 2$), both based on the outer pipe radius.

The boundary conditions (16) and (17) give

$$c_1 = c_2, \tag{19a}$$

$$\epsilon Pe_1 u_1 c_1 - \frac{\partial c_1}{\partial r} = \epsilon \phi \left(Pe_2 u_2 c_2 - \frac{\partial c_2}{\partial \eta} \right) = \mathcal{Q}, \tag{19b}$$

on $r = 1$, $\eta = 0$, where $\mathcal{Q} = \hat{\mathcal{Q}} \hat{L} / \hat{c}_0 \hat{D}_2$, and

$$c_2 = 0 \quad \text{on } \eta = 1. \tag{20}$$

In its present form, the complexity of Eqs. (18) does not lend itself to insightful analysis. However, in Sec. IV we exploit the small aspect ratio of the pipe to derive a simplified one-dimensional description for the radially averaged solute concentration by generalizing the results of classical Taylor-dispersion analysis.

IV. MODEL REDUCTION

Here we shall consider the behaviour of a pulse of solute whose extent is much smaller than the typical pipe length, but much larger than the pipe radius, in the spirit of classical Taylor-dispersion theory. To this end, we suppose the variations in solute concentration are characterized on a domain

size of order $\sqrt{\epsilon}$. It is thus convenient to convert to an appropriately scaled coordinate system, (ξ, τ), that advects with the mean axial velocity in the pipe:

$$z = z_0(\tau) + \sqrt{\epsilon}\xi, \tag{21a}$$

$$t = \tau, \tag{21b}$$

$$\frac{\mathrm{d}z_0}{\mathrm{d}\tau} = \overline{w}_1, \tag{21c}$$

where an overbar denotes the radial average,

$$\overline{w}_1(z,t) = 2\int_0^1 r w_1 \,\mathrm{d}r. \tag{22}$$

With respect to this coordinate system, (18a) becomes

$$\sqrt{\epsilon}Pe_1\left(\sqrt{\epsilon}\frac{\partial c_1}{\partial t} + \sqrt{\epsilon}u_1\frac{\partial c_1}{\partial r} + (w_1 - \overline{w}_1)\frac{\partial c_1}{\partial \xi}\right) = \frac{1}{r}\frac{\partial}{\partial r}\left(r\frac{\partial c_1}{\partial r}\right) + \epsilon\frac{\partial^2 c_1}{\partial \xi^2}. \tag{23}$$

From this point onwards we assume that Pe_i for $i = 1, 2$ are of order one. To leading order the concentration in the pipe is independent of r so we pose the expansion

$$c_1 = c_1^{(0)}(\xi,\tau) + \sqrt{\epsilon}c_1^{(1)}(r,\xi,\tau) + \epsilon c_1^{(2)}(r,\xi,\tau) + \ldots \tag{24}$$

and also expand

$$\begin{aligned} w_1(r,z,t) &= w_1(r, z_0(\tau) + \sqrt{\epsilon}\xi, \tau) \\ &= w_1(r, z_0(\tau), \tau) + \sqrt{\epsilon}\xi\frac{\partial w_1}{\partial z}(r, z_0(\tau), \tau) + \ldots, \end{aligned} \tag{25}$$

where w_1 has been solved for to leading order in (12b).

We consider first the transport in the pipe by setting $i = 1$. At $O(\sqrt{\epsilon})$, Eq. (23) gives

$$Pe_1\,(w_1 - \overline{w}_1)\frac{\partial c_1^{(0)}}{\partial \xi} = \frac{1}{r}\frac{\partial}{\partial r}\left(r\frac{\partial c_1^{(1)}}{\partial r}\right), \tag{26}$$

where w_1 and $\overline{w}_1$ are evaluated at $z = z_0(\tau)$. At $O(\epsilon)$ we find

$$Pe_1\left(\frac{\partial c_1^{(0)}}{\partial \tau} + \xi\frac{\partial w_1}{\partial z}\frac{\partial c_1^{(0)}}{\partial \xi} + (w_1 - \overline{w}_1)\frac{\partial c_1^{(1)}}{\partial \xi}\right) = \frac{1}{r}\frac{\partial}{\partial r}\left(r\frac{\partial c_1^{(2)}}{\partial r}\right) + \frac{\partial^2 c_1^{(0)}}{\partial \xi^2}, \tag{27}$$

which may be multiplied by r and integrated over the pipe cross-section $0 \le r \le 1$ to give

$$Pe_1\left(\frac{\partial c_1^{(0)}}{\partial \tau} + \xi\frac{\mathrm{d}\overline{w}_1}{\mathrm{d}z}\frac{\partial c_1^{(0)}}{\partial \xi} + 2\int_0^1 r\,(w_1 - \overline{w}_1)\frac{\partial c_1^{(1)}}{\partial \xi}\,\mathrm{d}r\right) = \left.\frac{\partial c_1^{(2)}}{\partial r}\right|_{r=1} + \frac{\partial^2 c_1^{(0)}}{\partial \xi^2}. \tag{28}$$

Equation (26) allows us to eliminate $c_1^{(1)}$ from (28) to give

$$Pe_1\left(\frac{\partial c_1^{(0)}}{\partial \tau} + \xi\frac{\mathrm{d}\overline{w}_1}{\mathrm{d}z}\frac{\partial c_1^{(0)}}{\partial \xi}\right) = \left.\frac{\partial c_1^{(2)}}{\partial r}\right|_{r=1} + \left(1 + Pe_1^2\mathcal{D}\right)\frac{\partial^2 c_1^{(0)}}{\partial \xi^2}, \tag{29}$$

where

$$\mathcal{D}(\tau) = 2\int_0^1 \left(\int_0^r \tilde{r}\,(w_1 - \overline{w}_1)\,\mathrm{d}\tilde{r}\right)^2 \frac{\mathrm{d}r}{r} \tag{30}$$

is the mechanical contribution to the dispersion as a result of the radial variations in the axial velocity. Use of (12b), (22), and (30) provides both the mean velocity and the mechanical diffusivity,

$$\overline{w}_1 = -\left(\frac{1}{8} + \frac{1}{2A(z)}\right)\frac{\mathrm{d}p_1}{\mathrm{d}z}, \tag{31a}$$

$$\mathcal{D} = \frac{1}{3072}\left(\frac{\mathrm{d}p_1}{\mathrm{d}z}\right)^2. \tag{31b}$$

We note that, in the limit of zero wall slip and wall permeability, $A \to \infty$ and (13) and (14) give $\mathrm{d}p_1/\mathrm{d}x = -8$ so that (31) recovers the classical Taylor-dispersion result, $\overline{w}_1 = 1$ and $\mathcal{D} = 1/48$.

To determine the diffusive flux across the interface, $\partial c_1^{(2)}/\partial r$ at $r = 1$, and close the problem we must consider the flux of solute transported across the pipe–membrane interface. Considering Eq. (18a) at leading order in ϵ gives

$$Pe_2 \frac{\partial}{\partial \eta}(u_2 c_2) = \frac{\partial^2 c_2}{\partial \eta^2}, \tag{32}$$

which upon integration with respect to η and application of (19b) yields

$$\phi\left(Pe_2 u_2 c_2 - \frac{\partial c_2}{\partial \eta}\right) = \mathcal{Q}(z,t). \tag{33}$$

Integrating once more, exploiting the fact that u_2 is constant across the membrane from (7) and applying the boundary condition (20) then gives

$$\mathcal{Q}(z,t) = \frac{\phi Pe_2 u_2}{1 - \exp(-Pe_2 u_2)} c_1|_{r=1}. \tag{34}$$

Substituting (34) into (19b) at $O(\epsilon)$ and use of (10d) and (19a) thus provides an expression for the required diffusive flux,

$$\left.\frac{\partial c_1^{(2)}}{\partial r}\right|_{r=1} = Pe_1 \gamma(\tau) c_1^{(0)}, \tag{35}$$

where $\gamma(\tau)$ is defined by

$$\gamma(\tau) = \frac{1}{2} \frac{\exp\left(\frac{\beta}{2}\frac{\mathrm{d}\overline{w}_1(z_0(\tau))}{\mathrm{d}z}\right)}{\exp\left(\frac{\beta}{2}\frac{\mathrm{d}\overline{w}_1(z_0(\tau))}{\mathrm{d}z}\right) - 1} \frac{\mathrm{d}\overline{w}_1(z_0(\tau))}{\mathrm{d}z}, \tag{36}$$

with $\beta = Pe_2/\phi$. Here we have also made use of the fact that $u_1(1,z,t) = \mathrm{d}\overline{w}_1/\mathrm{d}z$, obtained by radially averaging Eq. (2a). Hence, substituting this result into (29) we arrive at the governing equation for the leading-order solute concentration in the pipe and membrane, $C(\xi,\tau) = c_1^{(0)}(\xi,\tau) = c_2^{(0)}(\xi,\tau)$,

$$Pe_1\left(\frac{\partial C}{\partial \tau} + \xi \frac{\mathrm{d}\overline{w}_1(z_0(\tau),\tau)}{\mathrm{d}z}\frac{\partial C}{\partial \xi}\right) = \left(1 + Pe_1^2 \mathcal{D}(\tau)\right)\frac{\partial^2 C}{\partial \xi^2} - Pe_1 \gamma(\tau) C. \tag{37}$$

Equation (37) provides the generalization of the canonical Taylor-dispersion result to allow for radial outflow through a thin porous membrane. The result provides a dramatically simplified representation of the behaviour of solute within a particular flow field. The modification to the diffusivity, $\mathcal{D}$, due to the additional mechanical mixing contribution induced by the wall permeability is of particular interest since this plays a key role in the mobility of a solute within a given flow configuration. In the limit of zero wall slip and wall permeability, $A \to \infty$, $\mathcal{D} = 1/48$ and $\overline{w}_1 = 1$ so $\gamma(\tau) = 0$ and we obtain the result of standard Taylor dispersion.

Finally we consider the total solute delivered per unit length across the pipe–membrane interface, as a key parameter of interest in understanding and controlling solute dispersion. Rewriting the governing equation (37) in (z,t) coordinates enables us to identify the leading-order flux of solute transported through this wall as

$$\mathcal{R}(z,t) = -\left(2\frac{\mathrm{d}\overline{w}_1}{\mathrm{d}z} + (z - z_0)\frac{\mathrm{d}^2\overline{w}_1}{\mathrm{d}z^2} - \gamma(z,t)\right) C(z,t). \tag{38}$$

The total solute delivered per unit length across the pipe–membrane interface, $F(z)$, is then given by

$$F(z) = \int_{-\infty}^{\infty} \mathcal{R}(z,t)\,\mathrm{d}t. \tag{39}$$

In Sec. V we consider the effect of a spatially uniform wall permeability on the solute dispersion, before moving on to examine the appropriate strategy to determine the spatially dependent permeability required to provide a desired delivery of solute across the membrane in Sec. VI.

V. SOLUTE DISPERSION

A. Infinite tube

The effect of the permeability upon the solutal dispersion may be assessed by considering an infinitely long tube configuration. If the permeability is spatially uniform then both k and A are constant and (13) may be solved explicitly subject to (14) and the condition $p_1 \to 0$ as $z \to \infty$ to give

$$p_1(z) = \frac{8A}{(A+4)\lambda}\mathrm{e}^{-\lambda z}. \tag{40}$$

Here, for convenience, we have introduced the parameter λ, defined by

$$\lambda^2 = \frac{16\phi\alpha^2}{A(A+4)} = \frac{16\phi\alpha k}{(\alpha+4\sqrt{k})}, \tag{41}$$

which gives a measure of the membrane permeability, while A provides the wall slip at the membrane interface (weighted against the permeability). Equation (31) then provides the velocity and diffusivity,

$$\overline{w}_1 = \mathrm{e}^{-\lambda z}, \qquad \mathcal{D} = \frac{A^2}{48(A+4)^2}\mathrm{e}^{-2\lambda z}. \tag{42}$$

Substituting into (37) gives

$$\frac{\partial C}{\partial \tau} - \frac{\xi\lambda}{1+\lambda\tau}\frac{\partial C}{\partial \xi} = \frac{1}{Pe_1}\left(1 + \frac{Pe_1^2A^2}{48(A+4)^2(1+\lambda\tau)^2}\right)\frac{\partial^2 C}{\partial \xi^2} - \frac{\lambda C}{2(1+\lambda\tau)}\frac{\mathrm{e}^{-\frac{\beta\lambda}{2(1+\lambda\tau)}}}{1-\mathrm{e}^{-\frac{\beta\lambda}{2(1+\lambda\tau)}}}, \tag{43}$$

while (21) provides the relation between ξ and τ and the original coordinates:

$$\xi = \frac{z - \log(t+1)}{\sqrt{\epsilon}}, \qquad \tau = t. \tag{44}$$

We note that if we take the limit $\phi \to 0$ (so $\beta \to \infty$), and $k \to 0$ (so $\lambda \to 0$) we recover the classical Taylor-dispersion result for an impermeable tube.

The dispersive behaviour of a Gaussian pulse of solute delivered at $z = t = 0$ is examined in Figure 2 by solving (43) subject to the boundary conditions $C \to 0$ as $\xi \to \pm\infty$ and the initial condition

$$C(\xi, 0) = \frac{\omega}{\sqrt{\epsilon\pi}}\mathrm{e}^{-\omega^2\xi^2}, \tag{45}$$

where ω is an order-one parameter. Since the advection velocity relative to the peak, $-\xi\lambda/(1+\lambda\tau)$, is positive behind the peak (when $\xi < 0$) and negative in front (when $\xi > 0$), for non-zero wall permeabilities, this acts to counter the diffusive spreading. As the permeability is increased, the mean axial fluid advection speed and the solute concentration in the pulse within the pipe falls, as fluid is lost through the membrane. As a consequence, the extent of the dispersion is also reduced with increasing permeability, as observed in Figure 2(a). We note that, in the limit of an impermeable pipe, $\lambda = 0$, we must first take the limit $\beta \to \infty$, and so have shown graphs with varying λ for $\beta \to \infty$ to allow for a sensible comparison. It may be seen (by differentiation) that the

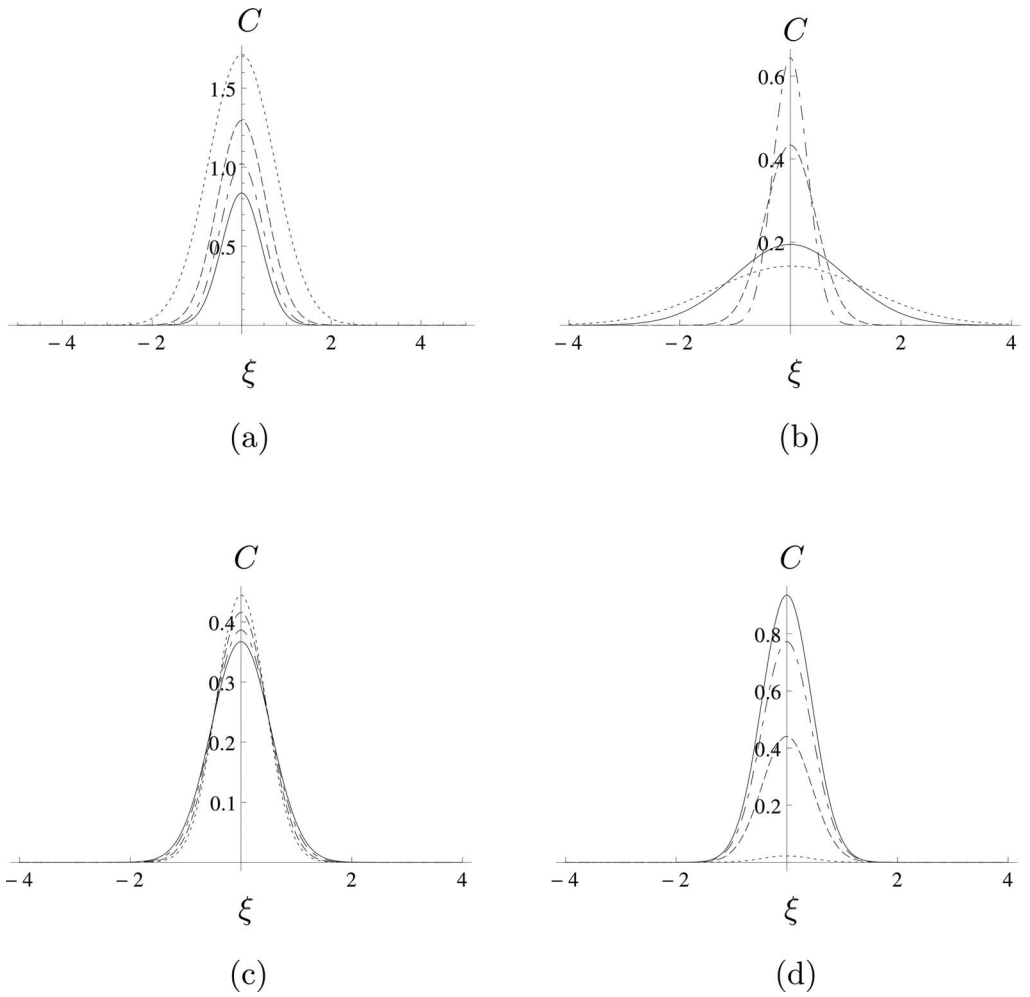

FIG. 2. Concentration profile, C, versus axial position, ξ, at time $t = 1$, for an initial distribution given by (45) with $\omega^2 = 10$ and $\epsilon = 0.1$. (a) $Pe_1 = 10$, $A = 1$, $\beta \to \infty$ and $\lambda = 1.2$ (solid), 0.8 (dotted-dashed), and 0.4 (dashed). The dotted line illustrates the classical Taylor-dispersion result for an impermeable pipe $\lambda = 0$. (b) $\lambda = 1$, $A = 1$, $\beta = 1$ and $Pe_1 = 500$ (solid), $8\sqrt{3}(A+4)/A$ when the dispersion is least pronounced (dotted-dashed), 10 (dashed), and 1 (dotted). (c) $\lambda = 1$, $Pe_1 = 10$, $\beta = 1$ and $A \to \infty$ (solid), 20 (dotted-dashed), 5 (dashed), and 0 (dotted). (d) $\lambda = 1$, $Pe_1 = 10$, $A = 1$ and $\beta \to \infty$ (solid), 5 (dotted-dashed), 2 (dashed), and 1 (dotted).

total effective diffusivity within the advecting reference frame,

$$\mathcal{D}_{\text{eff}} = \frac{1}{Pe_1}(1 + Pe_1\mathcal{D}) = \left(1 + \frac{Pe_1^2 A^2}{48(A+4)^2(1+\lambda\tau)^2}\right), \tag{46}$$

attains a minimum value when $Pe_1 = 1/\sqrt{\mathcal{D}}$, so the effect of dispersion at $\tau = 1$ is least pronounced for values of Pe_1 near $8\sqrt{3}(A+4)/A$ (Figure 2(b)). By comparison, varying the parameters A and β have, respectively, little, or zero, observed effect on the dispersion affecting only the peak height, which reduces with increasing A or increasing β (see Figures 2(c) and 2(d), respectively).

The total solute transported across the membrane per unit length, F, given by (39), is explored in Figure 3 for various values of λ, Pe_1, and β. Note that variations in the wall slip, A, have no impact on F, so that solute delivery to the membrane is independent of the slip parameter. (Consequently we do not present a counterpart to Figure 2 illustrating the effect of A on the flux, F.) As the membrane permeability is increased, so is the total solute delivery (observe Figure 3(a)); this behaviour is mimicked for increased supply of solute through an increase in Pe_1, and for an increase in the membrane porosity through a decrease in β (see Figures 3(b) and 3(c), respectively).

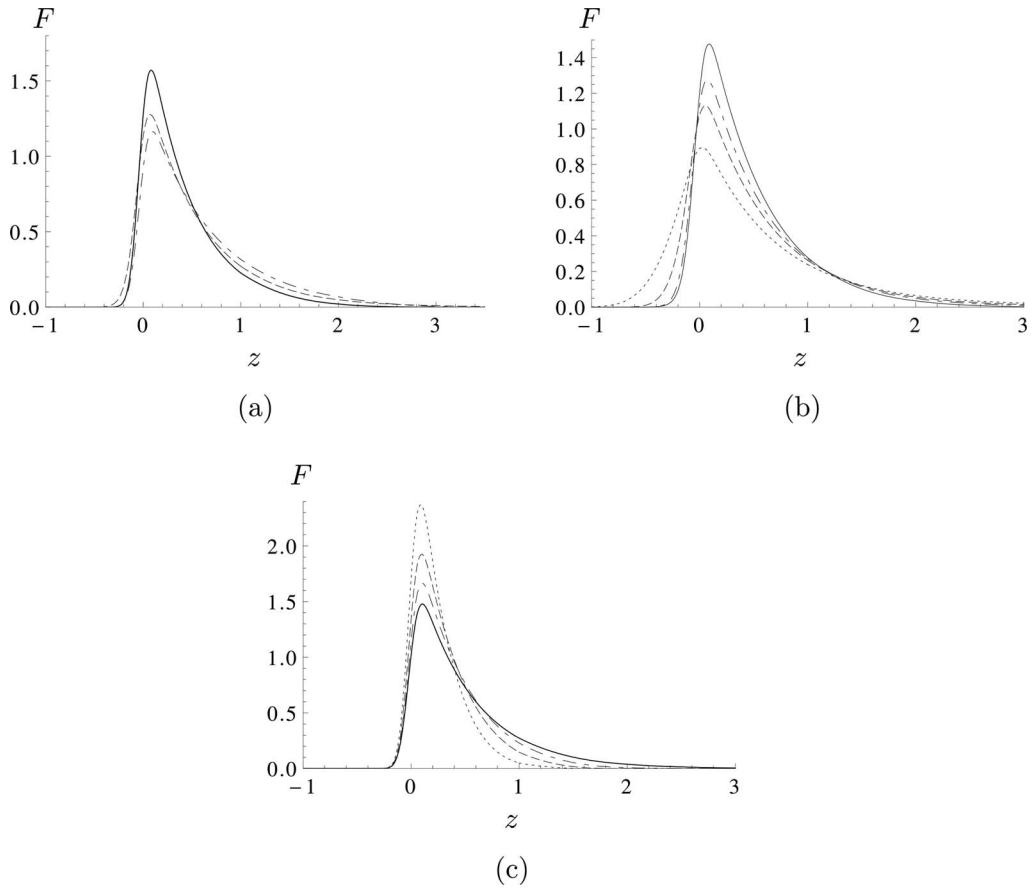

FIG. 3. Spatial dependence of total solute delivered through the side walls, F, given by (39) for an initial distribution given by (45) with $\omega^2 = 10$ and $\epsilon = 0.1$. (a) $Pe_1 = 10$, $A = 1$, $\beta \to \infty$ and $\lambda = 1.2$ (solid), 0.8 (dotted-dashed), and 0.4 (dashed). The dotted line illustrates the classical Taylor-dispersion result for an impermeable pipe, $\lambda = 0$. (b) $\lambda = 1$, $A = 1$, $\beta = 1$ and $Pe_1 = 200$ (solid), 1 (dotted-dashed), 0.5 (dashed), and 0.1 (dotted). (c) $\lambda = 1$, $A = 1$, $Pe_1 = 10$ and $\beta \to \infty$ (solid), 2 (dotted-dashed), 1 (dashed), and 0.5 (dotted).

B. Finite tube

Next we focus on a finite-tube set-up, motivated by the specific example of a tissue-engineering HFB. Tissue engineering involves the development of biological substitutes that restore, maintain, or improve tissue function or a whole organ.[20] This is normally achieved by culturing cells in a fluid-filled vessel (or bioreactor) in which the biochemical and biomechanical environment is controlled to promote growth of functional tissue. HFBs are one such bioreactor type that is designed specifically to enhance nutrient delivery to a cell population by using fluid flow to provide advective as well as diffusive transport. The flow set-up is accurately represented by the diagram in Figure 1, where the cells are seeded on the outer surface of the membrane (that is, on the surface $\hat{r} = \hat{R}_2$). Fluid containing nutrients is pumped down the tube, or *lumen*, in order to feed the cells, and the membrane also acts as a barrier that protects the cells from the direct effect of fluid shear. Ultimately the cells are harvested and implanted into a patient to replace tissue that has been damaged through age, trauma or disease.

The fluid transport problem in a HFB is adequately described by Sec. II; further information on the model set-up is provided in Shipley *et al.*[4] It is pertinent to understand how variations in the membrane permeability impact on nutrient delivery and cell population growth, so that these features can ultimately be predicted and controlled.

As for the infinite-pipe case, when the membrane permeability is spatially independent, k and A are both constant and Eq. (13) may be solved exactly subject to (14) and the condition

$p_1(1) = \mathcal{P}$, where $\mathcal{P}$ is a dimensionless measure of the pressure difference between the pipe outlet and atmospheric pressure. This gives

$$p_1 = \frac{\mathcal{P}\cosh(\lambda z)}{\cosh(\lambda)} + \frac{8A\sinh(\lambda(1-z))}{(A+4)\lambda\cosh(\lambda)}, \tag{47}$$

where λ is defined in (41). Equation (31) then provides

$$\overline{w}_1 = \frac{\cosh(\lambda(1-z))}{\cosh(\lambda)} - \frac{(A+4)\mathcal{P}\lambda\sinh(\lambda z)}{8A\cosh(\lambda)}, \tag{48a}$$

$$\mathcal{D} = \frac{\operatorname{sech}^2(\lambda)}{3072(A+4)^2}\left[(A+4)\mathcal{P}\lambda\sinh(\lambda z) - 8A\cosh(\lambda(1-z))\right]^2. \tag{48b}$$

When $\lambda = 0$ and the walls are impermeable the results (48a) reduce to standard Taylor dispersion for pipe flow. However, unlike in the case of an infinite pipe, the slip at the wall that arises through the parameter A now plays a role in the solute dispersion.

To ensure that we have an outflow at the end of the pipe for a given pressure $\mathcal{P}$, (48a) imposes a constraint on the maximum permeability $\lambda < \lambda^*$, where

$$\lambda^*\sinh(\lambda^*) = \frac{8A}{A+4}\frac{1}{\mathcal{P}}, \tag{49}$$

or conversely, for a given permeability λ, we must choose $\mathcal{P} \le \mathcal{P}^* = 8A/\lambda(A+4)\sinh(\lambda)$ to ensure an outflow at the end.

The dispersive behaviour of a localized pulse of solute upon injection at the pipe inlet is investigated by solving the system (21), (37), and (48) numerically subject to the conditions

$$C = \frac{\omega}{\sqrt{\epsilon\pi}}e^{-\omega^2 t^2/\epsilon} \quad \text{on } z = 0, \qquad \frac{\partial C}{\partial z} = 0 \quad \text{on } z = 1, \tag{50}$$

for $-\infty < t < \infty$, where ω is an order-one parameter. This corresponds to the injection of a Gaussian pulse at $z = 0$ with a peak concentration at $t = 0$ and width $O(\sqrt{\epsilon})$, with zero diffusive flux at the outlet. As for the case of an infinite tube, an increase in wall permeability reduces both the mean advection speed and the peak height (Figure 4(a)). Again, the dispersion of solute is a minimum when $Pe_1 = 1/\sqrt{\mathcal{D}(t)}$ (Figure 4(b)). However, unlike in the case of an infinite pipe, we are no longer able to obtain an explicit expression for $\mathcal{D}(t)$, although this may be determined implicitly using (21c) and (48). Although the apparent advection speed is independent of the Péclet number we also notice small adjustments in this upon variations in Pe_1, which arise as a result of the effect of the boundary at $z = 0$. Unlike for the case of an infinite pipe, dispersion now increases with decreasing A (note now we cannot choose $A = 0$ as this yields an unphysical velocity profile), although dispersion is unaffected by β: only the peak height is affected in this case, and reduces with increasing β (Figures 4(c) and 4(d)).

The total solute transported across the membrane per unit length, F, is explored in Figure 5. As would be expected, the flux of solute out of the sides of the domain through the membrane increases with increasing permeability, λ. However, we find that if we continue to increase the permeability then the total solute transported across the membrane at the downstream end lowers again. This occurs because, as the membrane permeability continues to increase, the solute is able to flow out of the wall earlier on, leaving less available solute for the later part of the pipe. This observation uncovers an interesting feature in the optimization problem for the solute distribution, which we study in more detail in Sec. VI. The flux out of the sides also increases with increasing Pe_1 and decreasing β although, as in the infinite-pipe case, A has very little effect on the solute transport.

VI. CONTROLLING THE SOLUTE DISTRIBUTION

A principal goal of the theory developed here is to provide a mechanism that allows us to choose the appropriate permeability to produce a desired (for example, uniform) spatial distribution in total

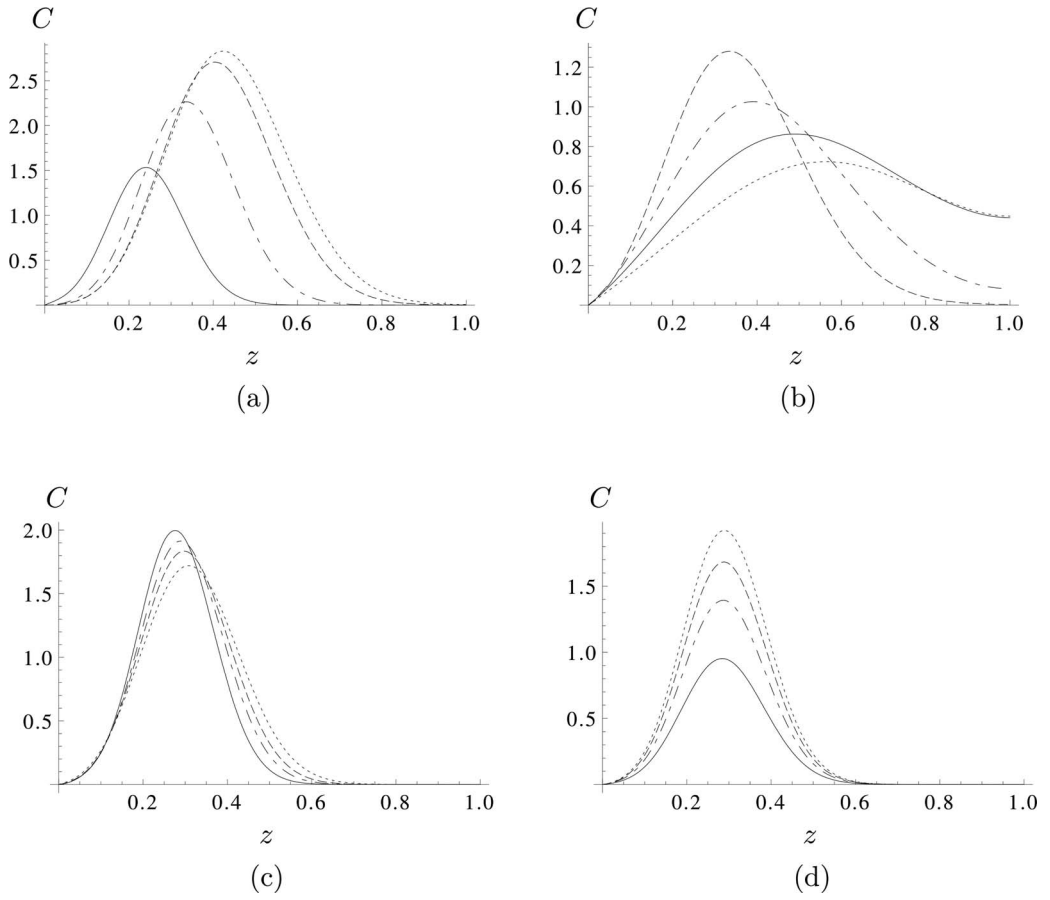

FIG. 4. Concentration profile, C versus axial position, z, at time $t = 0.4$ for a finite pipe with the initial distribution given by (45) and inlet and outlet conditions (50) with $\omega^2 = 10$ and $\epsilon = 0.1$. (a) $Pe_1 = 10$, $A = 1$, $\beta = 1$ and $\lambda = 1.2$ (solid), 0.8 (dotted-dashed), and 0.4 (dashed). The dotted line illustrates the classical Taylor-dispersion result for an impermeable pipe, $\lambda = 0$. (b) $\lambda = 1$, $A = 1$, $\beta = 1$ and $Pe_1 = 500$ (solid), 2 (dotted-dashed), 1 (dashed), and 0.5 (dotted). (c) $\lambda = 1$, $Pe_1 = 10$, $\beta = 1$ and $A \to \infty$ (solid), 20 (dotted-dashed), 5 (dashed), and 0.5 (dotted). (d) $\lambda = 1$, $Pe_1 = 10$, $A = 1$ and $\beta \to \infty$ (solid), 5 (dotted-dashed), 2 (dashed), and 0.5 (dotted).

solute delivered across the membrane, $F(z)$. By a change of variable, (39) may be written as

$$F = -\int_{-\infty}^{\infty} \frac{\sqrt{\epsilon}}{\overline{w}_1(z_0(\tau))} \left(2\frac{\mathrm{d}\overline{w}_1(z_0(\tau))}{\mathrm{d}z} + \sqrt{\epsilon}\xi \frac{\mathrm{d}^2\overline{w}_1(z_0(\tau))}{\mathrm{d}z^2} - \gamma(\tau) \right) C(\xi, \tau)\, \mathrm{d}\xi. \tag{51}$$

Since $C \ll 1$ when $\xi \gg 1$, the middle term in (51) will always be $\mathcal{O}\left(\sqrt{\epsilon}\right)$ smaller than the other two terms and may be neglected. Therefore

$$F = -\frac{\sqrt{\epsilon}}{\overline{w}_1(z_0(\tau))} \left(2\frac{\mathrm{d}\overline{w}_1(z_0(\tau))}{\mathrm{d}z} - \gamma(\tau) \right) \mathcal{C}, \tag{52}$$

where

$$\mathcal{C} = \int_{-\infty}^{\infty} C(\xi, \tau)\, \mathrm{d}\xi. \tag{53}$$

Integrating (37) by parts over $-\infty < \xi < \infty$ leads to

$$\frac{\partial \mathcal{C}}{\partial \tau} - \left(\frac{\mathrm{d}\overline{w}_1(z_0(\tau))}{\mathrm{d}z} - \gamma \right) \mathcal{C} = 0. \tag{54}$$

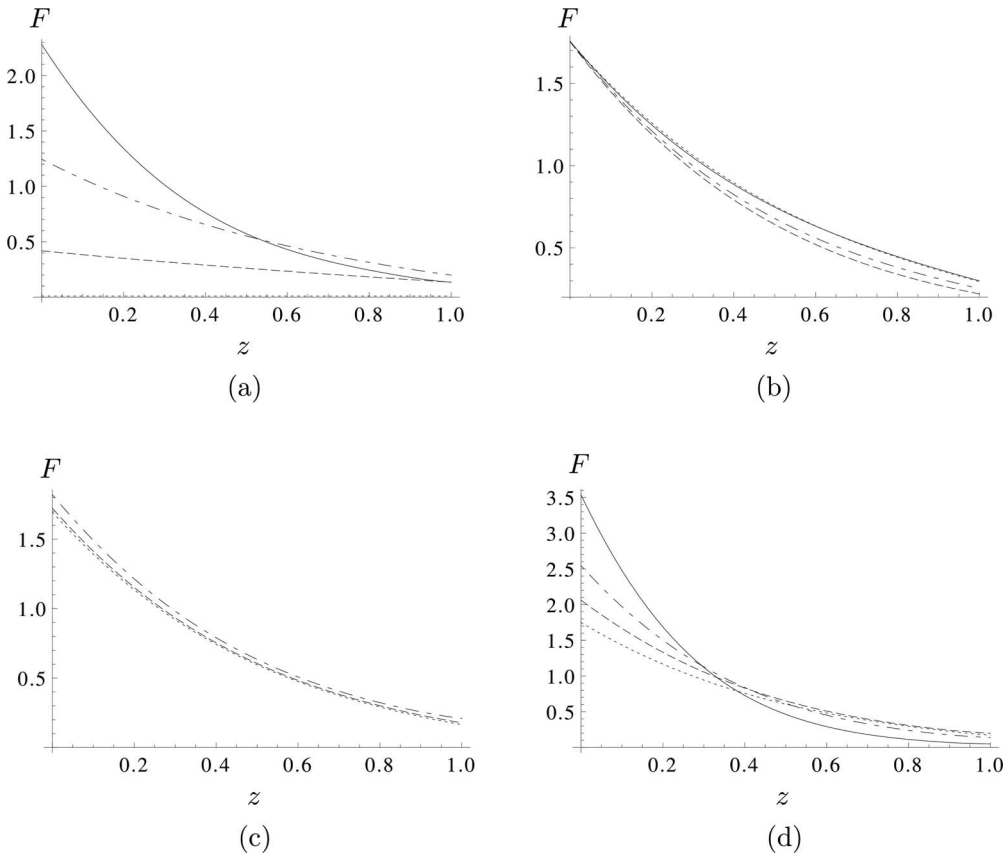

FIG. 5. Spatial dependence of total solute delivered through the side walls, F, given by (39) for a finite pipe with the inlet and outlet conditions (50) with $\omega^2 = 10$ and $\epsilon = 0.1$. (a) $Pe_1 = 10$, $A = 1$, $\beta = 1$ and $\lambda = 1.2$ (solid), 0.8 (dotted-dashed), 0.4 (dashed). The dotted line illustrates the classical Taylor-dispersion result for an impermeable pipe, $\lambda = 0$. (b) $\lambda = 1$, $A = 1$, $\beta = 1$ and (b) $Pe_1 = 200$ (solid), 2 (dotted-dashed), 1 (dashed), and 0.5 (dotted). (c) $\lambda = 1$, $Pe_1 = 10$, $\beta = 1$ and (a) $A \to \infty$ (solid), 20 (dotted-dashed), 5 (dashed), and 0.5 (dotted). (d) $\lambda = 1$, $Pe_1 = 10$, $A = 1$ and (a) $\beta \to \infty$ (solid), 5 (dotted-dashed), 2 (dashed), and 0 (dotted).

Equation (54) may be solved to give

$$\mathcal{C} = \frac{\overline{w}_1(z_0(\tau))}{\sqrt{\epsilon}} \exp\left(-\int_0^\tau \gamma(s)\,\mathrm{d}s\right), \tag{55}$$

since $\mathrm{d}z_0/\mathrm{d}\tau = \overline{w}_1(z_0(\tau))$ by (21), $\overline{w}_1(0) = 1$, and $\mathcal{C}(\xi, 0) = 1/\sqrt{\epsilon}$ using (45). Now,

$$\gamma = \frac{f\mathrm{e}^{-\beta f/2}}{2\left(1 - \mathrm{e}^{-\beta f/2}\right)}, \tag{56}$$

where

$$f(\tau) = -\frac{\mathrm{d}\overline{w}_1(z_0(\tau))}{\mathrm{d}z} \tag{57}$$

and therefore in (52) we have

$$F = \frac{\left(4 - 3\mathrm{e}^{-\beta f/2}\right) f}{2\left(1 - \mathrm{e}^{-\beta f/2}\right)} \exp\left[-\int_0^\tau \frac{f(s)\mathrm{e}^{-\beta f(s)/2}}{2(1 - \mathrm{e}^{-\beta f(s)/2})}\,\mathrm{d}s\right]. \tag{58}$$

We note that

$$\overline{w}_1 = \exp\left(-\int_0^\tau f(s)\,\mathrm{d}s\right), \tag{59}$$

which provides the relation between Lagrangian time τ and axial position z using (21),

$$z(\tau) = \int_0^{\tau} \exp\left(-\int_0^s f(v)\,\mathrm{d}v\right)\,\mathrm{d}s. \tag{60}$$

Further using (31), we may now express the pressure as

$$p_1(\tau) = \mathcal{P} + \int_{\tau}^{\tau^\star} \frac{8\alpha}{\alpha + 4\sqrt{k(s)}}\left[\exp\left(-\int_0^s f(u)\,\mathrm{d}u\right)\right]^2 \mathrm{d}s, \tag{61}$$

where $\tau^\star$ is given by

$$1 = \int_0^{\tau^\star} \exp\left(-\int_0^s f(u)\,\mathrm{d}u\right)\,\mathrm{d}s. \tag{62}$$

Finally, substituting (61) into (13) gives the following integro-differential equation for k,

$$\frac{\left(\alpha + 4\sqrt{k} - 32\alpha k\right)}{k^{3/2}(\alpha + 4\sqrt{k})^2}\frac{\mathrm{d}k}{\mathrm{d}\tau} + \frac{8\alpha f}{\alpha + 4\sqrt{k}} = \frac{16\alpha\phi k}{\alpha + 4\sqrt{k}}\left\{\mathcal{P} + \int_{\tau}^{\tau^\star} \frac{8\alpha}{\alpha + 4\sqrt{k}}\exp\left[-\int_0^s f(u)\,\mathrm{d}u\right]^2 \mathrm{d}s\right\}. \tag{63}$$

Thus, to achieve a desired final solute distribution $F(z)$, we use (58) and (60) to determine $f(\tau)$ and then determine $k(\tau)$ from (63). The result is then coupled with (60) to provide a parametric expression for the permeability, $k(z)$, required to achieve the required solute distribution.

When $\alpha \to \infty$ and the slip at the membrane surface is zero, (63) simplifies to provide an explicit representation for the required permeability,

$$k = \frac{f}{2\phi\left\{\int_{\tau}^{\tau^\star} 8\exp\left[-\int_0^s f(v)\,\mathrm{d}v\right]^2 \mathrm{d}s + \mathcal{P}\right\}}. \tag{64}$$

We note that, in this limit, we lose the freedom to apply an initial condition for k. This no-slip approximation has been shown to provide an accurate representation of specific membrane fabrication strategies for hollow-fibre bioreactor configurations.[4]

The most commonly desired situation is that in which the solute is transported through the membrane and distributed to the outer surface in a spatially uniform manner. In this case, $F = F^\star =$ constant. It is illuminating to consider the further simplified case when $\beta \to \infty$, and the effective boundary condition at the membrane wall corresponds to zero diffusive flux of solute. Such a set-up is also applicable in the case of a hollow-fibre bioreactor.[4] In this case, (58) becomes simply $f = F/2$, and so (60) reduces to

$$z = \frac{2}{F}\left(1 - \mathrm{e}^{-F\tau/2}\right), \tag{65}$$

which allows us to write the permeability, (64), explicitly in terms of z,

$$k = \frac{F}{4\phi\left[2F(z^2 - 1) + 8(1 - z) + \mathcal{P}\right]} \tag{66}$$

and illustrates the insight gained by this procedure.

Figure 6 shows the permeability required to achieve a spatially uniform distribution $F^\star$, for different values of $F^\star$, $\mathcal{P}$, α, and β. We note that, in the case of finite α, we must solve (63) and thus apply an appropriate initial condition, which we choose to ensure a physically sensible resulting permeability profile. As we would expect, the required permeability must increase as we move down the tube, to account for the reduction in available solute that arises as a result of its transport across the membrane earlier upstream. In addition, the increased permeability will allow for an increased flow rate into the membrane which will also contribute to enhancing the solute transport as we move farther downstream. This effect is shown to be amplified when any of $F^\star$, $\mathcal{P}$, α, or β are increased. For example, a higher trans-membrane pressure drop will require a greater increase in membrane permeability at the downstream compared to the upstream ends. An interesting observation is the

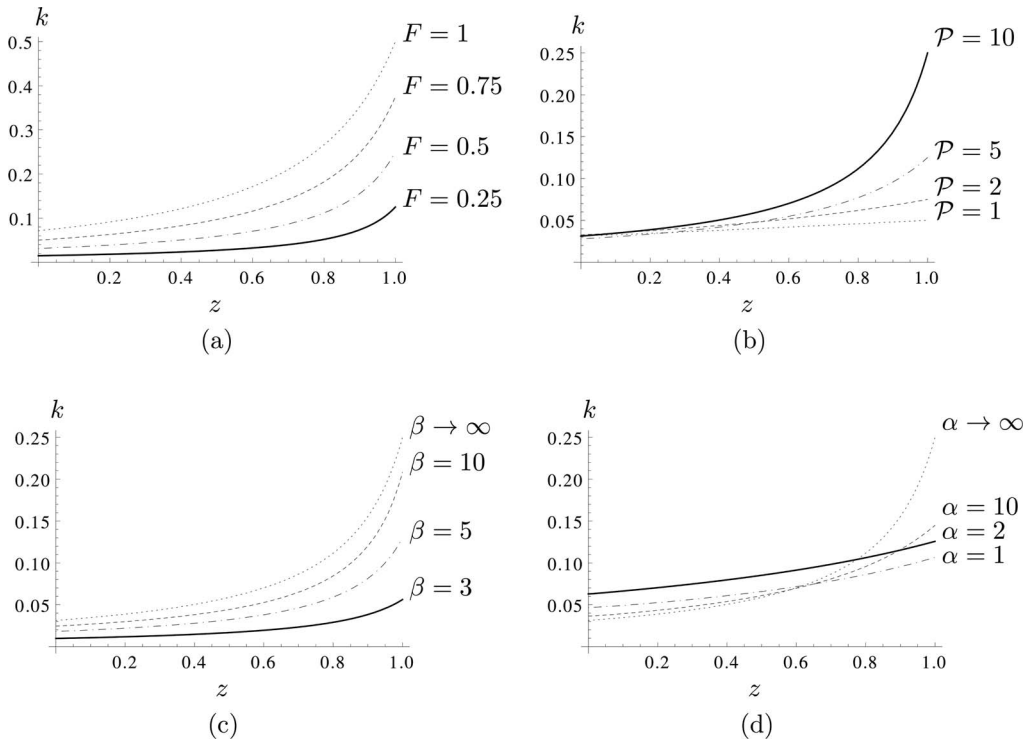

FIG. 6. Permeability, k versus space, z, required to achieve a spatially uniform distribution of solute across the membrane and the dependence upon (a) total proportion of solute transported across the membrane, $F^\star$, with α, $\beta \to \infty$ and $\mathcal{P} = 1$, given by (66); (b) outlet pressure, $\mathcal{P}$, with α, $\beta \to \infty$ and $F^\star = 0.5$, given by (66); (c) wall-condition parameter, β, with $\alpha \to \infty$, $\mathcal{P} = 1$ and $F^\star = 0.5$, given by (64); and (d) slip parameter, α, with $\beta \to \infty$, $\mathcal{P} = 1$ and $F^\star = 0.5$, given by (63).

effect of an increase in slip at the membrane wall (demonstrated by a reduction in α) for which the necessary spatial variations in permeability required to generate such a uniform solute distribution are less pronounced. This suggests that those membranes that offer a non-zero slip at the interface may be more conducive in generating a uniform solute distribution, and thus may offer a potential design criterion for membrane fabrication.

Equations (13) and (31) provide the corresponding pressure profile, velocity profile, and mechanical dispersion for a set-up with a permeability (66) for which the solute distribution generated is spatially uniform:

$$p_1 = \mathcal{P} + 8(1 - z) - 2F^\star(1 - z^2), \tag{67}$$

$$\overline{w}_1 = 1 - \frac{F}{2}z, \tag{68}$$

$$\mathcal{D} = \frac{1}{48}\left(1 - \frac{F}{2}z\right)^2. \tag{69}$$

We observe that all of the supplied solute is delivered across the walls (that is, $F^\star = 1$) when the mean flow at the outlet is half that of the inlet. The allowance of solute outflow produces an interesting modified mechanical dispersion term that reduces with axial distance down the pipe.

VII. CONCLUSIONS

Solute transport in a tube comprising thin porous walls is a scenario that arises in a spectrum of important applications ranging from the environment to biology. Two key areas are cross-flow filtration (used for water purification, protein separation for gene therapies, blood fractionation, and tissue

engineering) and field-flow fractionation devices (used in the separation and size characterization of particulates, water-soluble polymers, and biological macromolecules). An issue that currently limits device design is a fundamental understanding of the relationship between the controllable system features and the resulting solute distribution. In this paper we addressed this by exploring the link between membrane permeability and solute delivery.

A reduced asymptotic one-dimensional model that characterizes the dispersive behaviour of a pulse of solute when injected into a long thin porous-walled tube was derived. The resulting diffusion coefficient provides a generalization of the standard Taylor–Aris dispersion coefficient that arises for flow in a pipe with impermeable walls. The consequent additional dispersion was found to reduce both with increasing permeability and with axial distance down the tube, reaching zero at the outlet when the flow velocity here is zero and all fluid transport takes place across the membrane.

The effect of a permeable wall upon the solute dispersion was clearly apparent, with the concentration of solute falling more quickly and advecting more slowly in pipes with a greater wall permeability. However, as the solute propagates down the tube the diffusivity is reduced from the value anticipated by Taylor-dispersion theory for an impermeable pipe.

The use of a spatially dependent membrane permeability was explored to exploit the observed features to control the solute distribution. A strategy for determining the wall permeability required to generate a given solute axial distribution was derived which was shown to possess an explicit analytic solution in the case of a uniform final solute distribution with zero slip and diffusive solute flux at the membrane wall, a regime that has been shown to be applicable in hollow-fibre bioreactor configurations. Interestingly, as the membrane slip increases, the applied pressure gradient required to achieve a uniform distribution of solute is reduced, and the spatial variations in the permeability are also less pronounced. Achieving large spatial variations in membrane permeability can be complex in practice, so this result provides an appealing strategy for membrane design in which a spatially uniform solute transport is induced for minimum spatial variations in the membrane permeability.

The analysis and results presented here provide new insights into the correlation between membrane permeability, dispersion, and solute delivery, and thus can be used to inform membrane design in the future.

ACKNOWLEDGMENTS

This publication is based on work partially supported by Award No. KUK-C1-013-04, made by King Abdullah University of Science and Technology (KAUST). The authors gratefully acknowledge helpful discussions with Dr. Y. Davit, Dr. M. Taroni, Dr. D. Vella, and Professor H. A. Stone.

[1] H. W. Hou, A. A. S. Bhagat, W. C. Lee, S. Huang, J. Han, and C. T. Lim, "Microfluidic devices for blood fractionation," Micromachines **2**(3), 319–343 (2011).
[2] R. S. Juang, H. L. Chen, and Y. S. Chen, "Resistance-in-series analysis in cross-flow ultrafiltration of fermentation broths of *Bacillus subtilis* culture," J. Membr. Sci. **323**(1), 193–200 (2008).
[3] S. Metsamuuronen, J. Howell, and M. Nystrom, "Critical flux in ultrafiltration of myoglobin and baker's yeast," J. Membr. Sci. **196**(1), 13–25 (2002).
[4] R. J. Shipley, S. L. Waters, and M. J. Ellis, "Definition and validation of operating equations for poly(vinyl alcohol)-poly(lactide-co-glycolide) microfiltration membrane scaffold bioreactors," Biotechnol. Bioeng. **107**, 382–392 (2010).
[5] T. Vicente, C. Peixoto, M. J. T. Carrondo, and P. M. Alves, "Purification of recombinant baculoviruses for gene therapy using membrane processes," Gene Ther. **16**(6), 766–775 (2009).
[6] J. C. Giddings, "Field-flow fractionation," Sep. Sci. Technol. **19**(11–12), 831–847 (1984).
[7] A. Litzen and K. G. Wahlund, "Improved separation speed and efficiency for proteins, nucleic acids and viruses in asymmetrical flow field flow fractionation," J. Chromatogr. A **476**, 413–421 (1989).
[8] M. H. Moon, I. Park, and Y. Kim, "Size characterization of liposomes by flow field-flow fractionation and photon correlation spectroscopy: Effect of ionic strength and pH of carrier solutions," J. Chromatogr. A **813**(1), 91–100 (1998).
[9] W. J. Lee, B. R. Min, and M. H. Moon, "Improvement in particle separation by hollow fiber flow field-flow fractionation and the potential use in obtaining particle size distribution," Anal. Chem. **71**(16), 3446–3452 (1999).
[10] S. R. Raine, W. S. Meyer, D. W. Rassam, J. L. Hutson, and F. J. Cook, "Soil–water and solute movement under precision irrigation: knowledge gaps for managing sustainable root zones," Irrig. Sci. **26**(1), 91–100 (2007).
[11] J. M. MacDonald, S. P. Wolfe, R. I. Chowdhury, H. Kubota, and L. M. Reid, "Effect of flow configuration and membrane characteristics on membrane fouling in a novel multicoaxial hollow-fiber bioartificial liver," Ann. N.Y. Acad. Sci. **944**(1), 334–343 (2001).

[12] N. S. Hanspal, A. N. Waghode, V. Nassehi, and R. J. Wakeman, "Development of a predictive mathematical model for coupled Stokes/Darcy flows in cross-flow membrane filtration," Chem. Eng. J. **149**(1–3), 132–142 (2009).
[13] L. Huang and M. T. Morrissey, "Finite element analysis as a tool for crossflow membrane filter simulation," J. Membr. Sci. **155**(1), 19–30 (1999).
[14] R. P. Ma, C. H. Gooding, and W. K. Alexander, "A dynamic model for low-pressure, hollow-fiber ultrafiltration," AIChE J. **31**(10), 1728–1732 (1985).
[15] S. W. Yuan and A. B. Finkelstein, "Laminar pipe flow with injection and suction through a porous wall," Trans. ASME **78**, 719 (1956).
[16] M. R. Doshi, W. N. Gill, and R. Shankar Subramanian, "Unsteady reverse osmosis or ultrafiltration in a tube," Chem. Eng. Sci. **30**(12), 1467–1476 (1975).
[17] G. S. Beavers and D. D. Joseph, "Boundary conditions at a naturally permeable wall," J. Fluid Mech. **30**(1), 197–207 (1967).
[18] A. S. Berman, "Laminar flow in channels with porous walls," J. Appl. Phys. **24**, 1232–1235 (1953).
[19] R. J. Shipley and S. L. Waters, "Fluid and mass transport modelling to drive the design of cell-packed hollow fibre bioreactors for tissue engineering applications," Math. Med. Biol. **29**, 329–359 (2012).
[20] R. Langer and J. P. Vacanti, "Tissue engineering," Science **260**(5110), 920–926 (1993).